*International Journal of Innovative Computing, Information and Control*
Volume **12**, Number **4**, August **2016**

ICIC International ©2016 ISSN 1349-4198
pp. 1271–1286

# NUMERICAL SIMULATION ON THE INFLUENCES OF CYLINDERICAL OBSTACLES ON OVERPRESSURE AND TEMPERATURE OF NATURAL GAS EXPLOSION IN MIDDLE DECK OF OFFSHORE OIL PLATFORM

Pengcheng Wang[1,*] and Hongru Zhao[2]

[1]Marine Engineering College
Dalian Maritime University
No. 1, Linghai Road, Dalian 116026, P. R. China
*Corresponding author: wpc6688@163.com

[2]Henry Samueli School of Engineering and Applied Science
University of California – Los Angeles
Los Angeles, California 90095, United States
hrzhao@ucla.edu

Received January 2016; revised May 2016

Abstract. *Natural gas explosions on offshore oil platforms can lead to serious accidents and damage to property, both of which necessitate the study on how to reduce the damage. The quantity of devices and the volumetric blockage ratio of equipment have a huge impact on peak overpressure and temperature, and these can even directly influence the consequences of accidents. In order to research rules of peak overpressure and temperature caused by natural gas explosion in differently obstructed situations in the middle deck of offshore oil platform, AutoReaGas, a widely known gas explosion simulative software and the finite element analysis method have been used. We design twelve numerical simulative models in the case of cylindrical obstacles to study rules of peak overpressure and temperature in natural gas explosions, which are influenced by different quantities and volumetric blockage ratio of obstacles. The research results show that the peak overpressure increases with the volumetric blockage ratios of cylindrical obstacles. However, the influence by quantities of obstacles decreases with the increasing of volumetric blockage ratio. Furthermore, there is a peak temperature range of 1900-2700K caused by natural gas explosion in the middle deck. The influence of the volumetric blockage ratio is smaller compared with the quantities of obstacles and the amplitude is less than 100K when obstacles are not less than eight. The research could not only provide reference to the reasonable layout of equipment on the offshore oil platform, but also provide the certain theoretical basis for the investigation and analysis of similar accidents.*
**Keywords:** Natural gas explosion, Overpressure, Offshore oil platform, Cylindrical obstacle, Volumetric blockage ratio

1. **Introduction.** Offshore oil exploitation has been substantially increasing worldwide over recent years due to economic development and national policies. It is well known that offshore oil exploitation has great risk which may lead to unacceptable disaster, especially in cases of fires and explosions. For example, the accidents that happened on Piper Alpha platform in Britain, "deep horizon" drilling platform in Mexico, and the floating production, storage and unloading tanker (FPSO) in Brazil all caused severe property damage and brought hazards to the marine environment. A method to reduce loss and damage caused by such accidents has attracted a lot of attention in both the research community and the industry recently [1], and many efforts have been undertaken to study after-explosion shock wave overpressure and temperature. Li et al. [2] and Ibrahim

and Masri [3] studied the relationship between obstacles and flammable gas explosions by using numerical simulation and experimental methods respectively. They pointed out that as the obstacles get bigger, the shock wave peak overpressure grows higher. Salzano et al. [4] reported gas explosion with circular obstacles and assessed the ability of AutoReaGas to simulate the gas explosion behavior in obstructed environments. Zhang et al. [5] analyzed the coupling relation between the overpressure and high temperature. Mercx et al. [6] applied the TNT equivalency method and the TNO multi-Energy method to calculating the explosion blast load on an offshore platform. Pang et al. [7] studied the dependence of explosion shock wave on support. The results show different support spacing can have great impact on overpressure and impulse. Graham et al. [8] researched the explosions in which flame acceleration appears to have been driven by the congestion and confinement provided by closely spaced tankers or other heavy goods vehicles, and these are as the function of obstacles to influence the overpressure and temperature [9]. In order to study the influence by obstacles, the shape, position and quantity of the obstacles should be considered. However, most of the research focuses on the planar geometry structure, such as the repetition barrier, the barrier ring, and the sector plate. In practice, most of the obstacles are three-dimensional structures, complex shapes and many in quantity. Therefore, studying the rules of temperature and peak overpressure has practical value, which is influenced by stereo and multiple obstacles. This paper establishes different offshore oil platform models with cylindrical obstacles, with analysis through AutoReaGas and the finite element method [10,11]. The cylindrical obstacles are located on the middle deck of offshore oil platform and these are sited in different positions and vary by volume. The rules of peak temperature and overpressure are analyzed in different obstructed conditions, which could be used to optimize the layout of equipment and minimize the loss caused by natural gas explosions.

2. **Basic Computational Formulas and Equations.** AutoReaGas uses the finite element computation and analysis method to solve many problems relating to gas explosions and blasts. The gas dynamic is described by conservation equations for mass, momentum and energy. They are as follows [12]:
The mass equation

$$\frac{\partial \rho}{\partial t} + \frac{\partial}{\partial x_i}(\rho u_i) = 0 \tag{1}$$

The momentum equation

$$\frac{\partial}{\partial t}(\rho u_i) + \frac{\partial}{\partial x_j}(\rho u_i u_j) = \frac{\partial \tau_{ij}}{\partial x_j} - \frac{\partial P}{\partial x_i} \tag{2}$$

The energy equation

$$\frac{\partial}{\partial t}(\rho E) + \frac{\partial}{\partial x_j}(\rho u_j E) = \frac{\partial}{\partial x_j}\left(\Gamma_E \frac{\partial E}{\partial x_j}\right) - \frac{\partial}{\partial x_j}(\rho u_j) + \tau_{ij}\frac{\partial u_i}{\partial x_j} \tag{3}$$

The fuel mass fraction equation

$$\frac{\partial}{\partial t}(\rho Y_{fu}) + \frac{\partial}{\partial x_j}\left(\rho u_j Y_{fu} - \Gamma_{fu}\frac{\partial Y_{fu}}{\partial x_j}\right) = R_{fu} \tag{4}$$

The turbulence model includes the turbulence equation ($\kappa$ equations) and the dissipation rate transport equation ($\varepsilon$ equations), the specific forms of which are as follows:
The $\kappa$ equation is

$$\frac{\partial}{\partial t}(\rho k) + \frac{\partial \kappa}{\partial x_j}(\rho u_j k) = \frac{\partial}{\partial x_j}\left(\Gamma_k \frac{\partial k}{\partial x_j}\right) + \tau_{ij}\frac{\partial u_i}{\partial x_j} - \rho\varepsilon \tag{5}$$

The $\varepsilon$ equation is

$$\frac{\partial}{\partial t}(\rho\varepsilon) + \frac{\partial}{\partial x_j}\left(\rho u_j \varepsilon - \Gamma_\varepsilon \frac{\partial \varepsilon}{\partial x_j}\right) = C_1 \frac{\varepsilon}{\kappa}\tau_{ij}\frac{\partial u_i}{\partial x_j} - C_2\rho\frac{\varepsilon^2}{\kappa} \tag{6}$$

where

$$\tau_{ij} = \mu_t\left(\frac{\partial u_i}{\partial x_j} + \frac{\partial u_j}{\partial x_i}\right) - \frac{2}{3}\delta_{ij}\left(\rho\kappa + \mu_t\frac{\partial u_j}{\partial x_j}\right) \tag{7}$$

$x_i$ is the space coordinate in the direction of $i$, $\rho$ is density, $u_i$ is particle velocity, $p$ is static pressure, $E$ is energy ($C_V T + Y_{mf} H_C = energy$), $k$ is turbulent kinetic energy, $\varepsilon$ is dispassion rate of turbulent kinetic energy, $Y_{fu}$ is fuel mass fraction, $\mu_t$ is turbulent viscosity coefficient, $R_{fu}$ is volumetric combustion rate, $\Gamma_E$ is energy dissipation rate coefficient of turbulent flow, $\Gamma_{fu}$ is fuel dissipation coefficient of turbulent flow, $C_1$ is model constant, $C_2$ is model constant, $C_V$ is specific heat (constant volume), $T$ is temperature, $H_c$ is heat of combustion of fuel, and $\delta_{ij}$ is Kronecker delta.

A large body of experimental data on turbulent flame propagation is correlated by Bray [13], which is in the empirical relationship between the speed of turbulent, turbulent parameters and mixture properties.

$$S_t = 1.8u^{'0.412}.L_t^{0.196}.S_l^{0.784}.\nu^{-0.196} \tag{8}$$

where $S_t$ is the turbulent burning speed, $u'$ is the turbulent intensity, $L_t$ is the turbulence characteristic length scale (integral scale), $S_l$ is laminar burning velocity flammable mixture and $\nu$ is the kinematic viscosity of the unburned flammable mixture. The effect of temperature, pressure and front wrinkling of flame on the laminar burning velocity are described by a second adjustable parameter $F_s$ which relates $S_b$ to the flame radius $r_m$ and to the theoretical laminar flame speed as follows:

$$S_b = S_1\left(1 + F_s r_m\right) \tag{9}$$

The constants used for simulations of premixed gas explosions are given in Table 1.

TABLE 1. The set of constants used for simulation

| *Variable* | *Value* |
|---|---|
| *Gamma* | *1.25* |
| *Methane composition (% volume)* | *9.5%* |
| *Heat of combustion* | $2.751 \times 10^6 J/kg$ |
| *Lower flammable limit (% mass)* | *2.82%* |
| *Upper flammable limit (% mass)* | *8.87%* |
| *Burning velocity* | $0.45 m/s$ |
| *Flame speed factor* | *0.15* |
| *Viscosity* | $2.5 \times 10^{-5} Ns/m^2$ |
| *Turbulent combustion modelling constant* | *70* |

3. **Modeling and Simulative Conditions.** This paper applies AutoReaGas software which has high precision and accuracy in gas explosion simulation. It has been widely used around the world, including in marine equipment (Platform, EPSO) and shore facilities (Chemical pharmaceutical and Power plants, Mining and Transportation), especially within the field of safety and risk analysis for consultants, contractors, operators and researchers. The reliability of AutoReaGas has been verified, as the simulation prediction and test results are better in the famous BFETS test.

3.1. **Numerical model.** The offshore oil platform model constructed in AutoReaGas is shown in Figure 1. The computational domain of the middle deck model is 50m × 50m × 5m along the $x$, $y$, and $z$ axes in Cartesian coordinates. The ignition source is in the center of the domain at $(0, 0, 0)$. Obstacles are distributed equidistant along the circumference of circles with radii of 5 meters, 10 meters, 15 meters, and 20 meters from the ignition

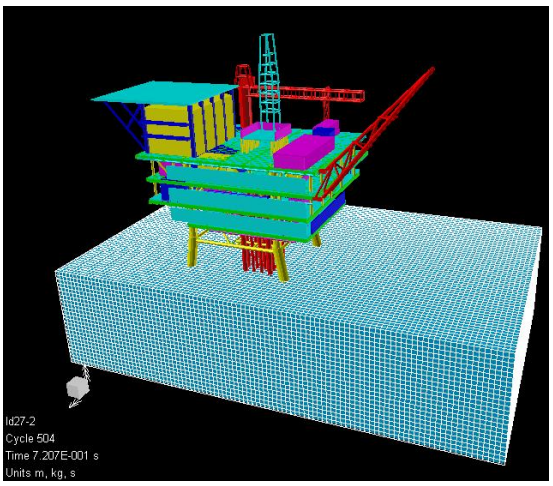


FIGURE 1. Whole offshore oil platform model

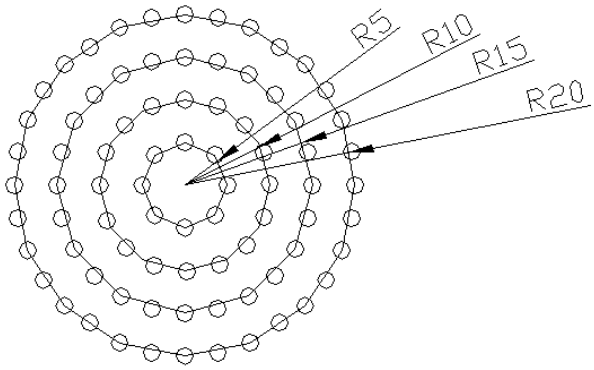


FIGURE 2. Cylindrical obstacles' positions in the middle deck of offshore oil platform

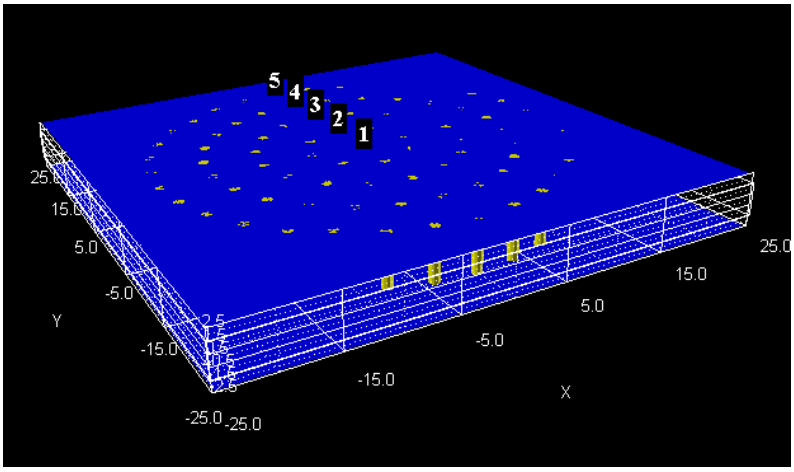


FIGURE 3. Gauged points and boundary

source (see Figure 2). The gas to be detonated is a mixture of 9.5% methane and 90.5% air, which is the stoichiometric concentration distributed normally in the computational domain. The initial temperature is 300K and the atmospheric pressure is $1.025 \times 10^5$pa. Initial velocities of natural gas and environmental wind are 0m/s.

TABLE 2. Working conditions of simulation

| working condition | R = 10m, H = 5m | | | R = 10m, H = 5m | | | R = 15m, H = 5m | | | R = 20m, H = 5m | | | Ra |
|---|---|---|---|---|---|---|---|---|---|---|---|---|---|
| | Q | r | V ($m^3$) | Q | r | V ($m^3$) | Q | r | V ($m^3$) | Q | r | V ($m^3$) | % |
| *MAO* | *0* | *NA* | *NA* | *0* | *NA* | *NA* | *0* | *NA* | *NA* | *0* | *NA* | *NA* | *0* |
| *MCY1* | *8* | *0.5* | *3.9* | *0* | *NA* | *NA* | *0* | *NA* | *NA* | *0* | *NA* | *NA* | *0.2* |
| *MCY2* | *8* | *0.5* | *3.9* | *16* | *0.5* | *3.9* | *0* | *NA* | *NA* | *0* | *NA* | *NA* | *0.7* |
| *MCY3* | *8* | *0.5* | *3.9* | *16* | *0.5* | *3.9* | *24* | *0.5* | *3.9* | *0* | *NA* | *NA* | *1.5* |
| *MCY4* | *8* | *0.5* | *3.9* | *16* | *0.5* | *3.9* | *24* | *0.5* | *3.9* | *32* | *0.5* | *3.9* | *2.5* |
| *MCY5* | *8* | *1* | *15.9* | *0* | *NA* | *NA* | *0* | *NA* | *NA* | *0* | *NA* | *NA* | *1.0* |
| *MCY6* | *8* | *1* | *15.9* | *16* | *1* | *15.9* | *0* | *NA* | *NA* | *0* | *NA* | *NA* | *3.1* |
| *MCY7* | *8* | *1* | *15.9* | *16* | *1* | *15.9* | *24* | *1* | *15.9* | *0* | *NA* | *NA* | *6.1* |
| *MCY8* | *8* | *1* | *15.9* | *16* | *1* | *15.9* | *24* | *1* | *15.9* | *32* | *1* | *15.9* | *10.2* |
| *MCY9* | *8* | *1.5* | *34.9* | *0* | *NA* | *NA* | *0* | *NA* | *NA* | *0* | *NA* | *NA* | *2.2* |
| *MCY10* | *8* | *1.5* | *34.9* | *16* | *1.5* | *34.9* | *0* | *NA* | *NA* | *0* | *NA* | *NA* | *6.7* |
| *MCY11* | *8* | *1.5* | *34.9* | *16* | *1.5* | *34.9* | *24* | *1.5* | *34.9* | *0* | *NA* | *NA* | *13.4* |
| *MCY12* | *8* | *1.5* | *34.9* | *16* | *1.5* | *34.9* | *24* | *1.5* | *34.9* | *32* | *1.5* | *34.9* | *22.3* |

*Notes: "R" represents the distance between the ignition source and the center of obstacle, "H" represents the height of obstacle, "V" represents the volume of obstacle, "Q" represents the quantity of obstacles, "r" represents the radius of cylindrical obstacle, and "Ra" represents the volumetric blockage ratio*

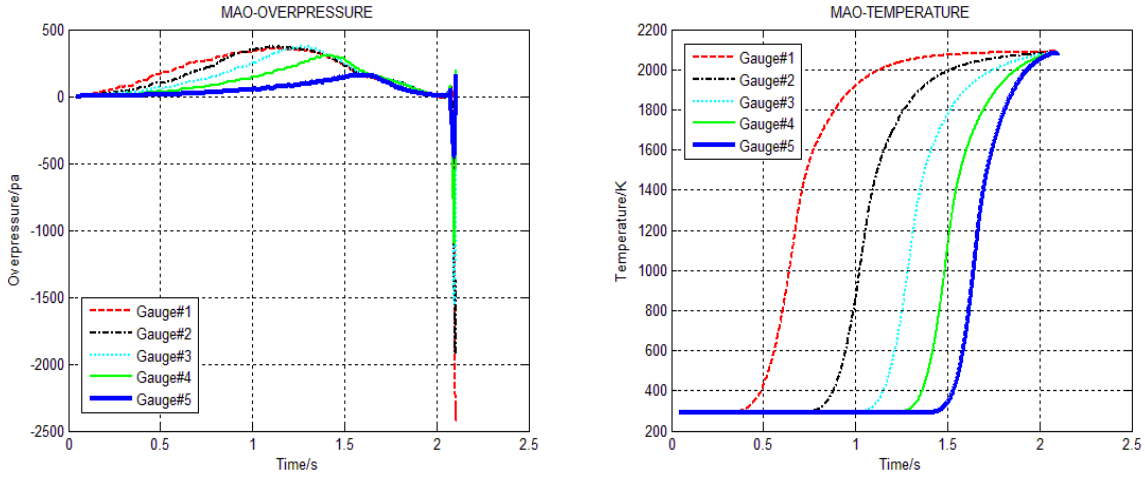


(a) (b)

FIGURE 4. Two charts of overpressure and temperature without any obstacle (a) the relationship between overpressure and time in five gauged positions, (b) the relationship between temperature and time in five gauged positions

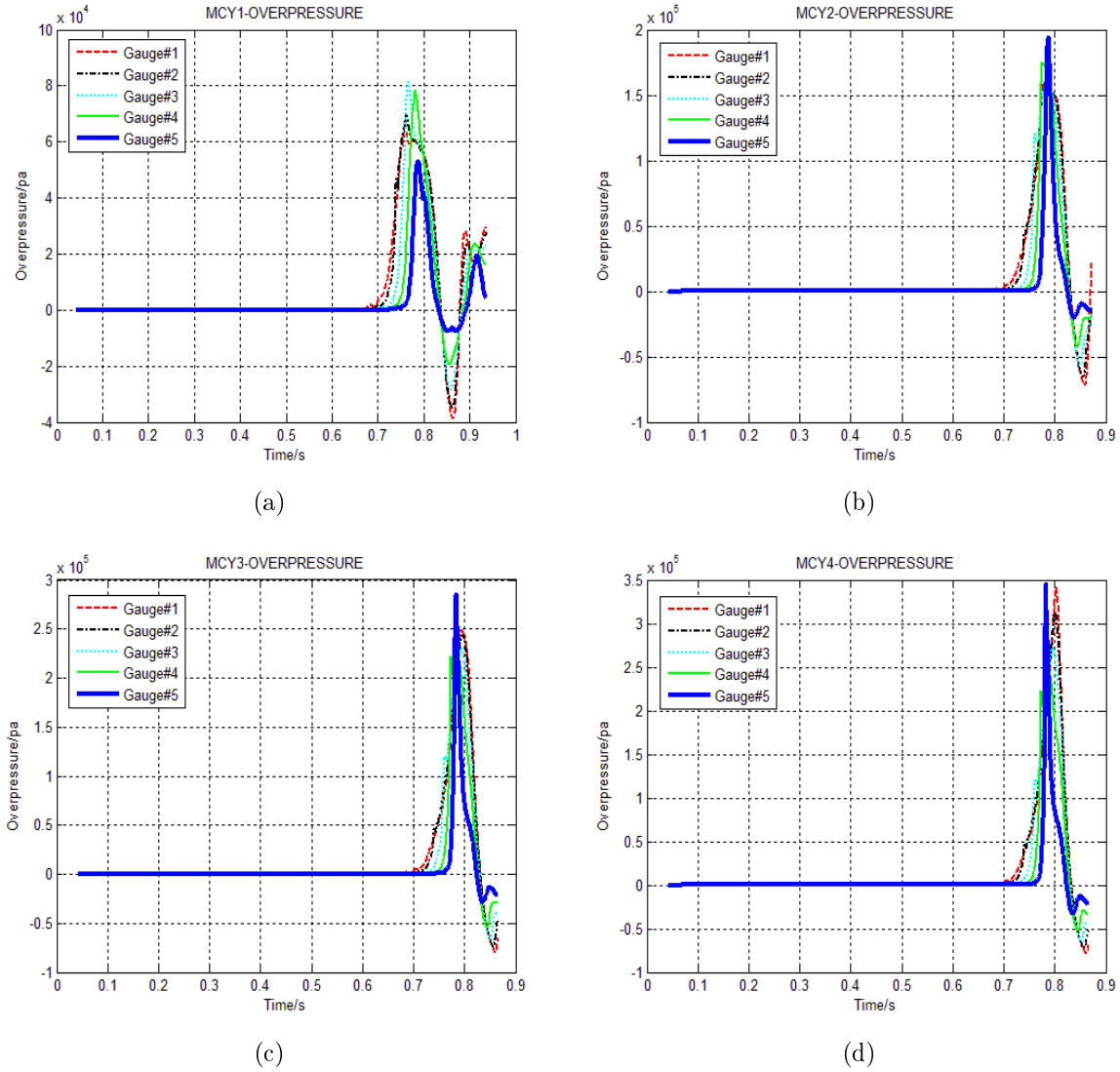


FIGURE 5. The overpressure is influenced by the quantities of cylindrical obstacles and the volume of each is $3.9\text{m}^3$. (a) 8 obstacles distribute in the circle of R = 5m ($\text{MCY}_1$), (b) 8 cylindrical obstacles distribute in the circle of R = 5m, and 16 cylindrical obstacles distribute in the circle of R = 10m ($\text{MCY}_2$), (c) 8 cylindrical obstacles distribute in the circle of R = 5m, 16 cylindrical obstacles distribute in the circle of R = 10m, and 24 cylindrical obstacles distribute in the circle of R = 15m ($\text{MCY}_3$), (d) 8 cylindrical obstacles distribute in circle of R = 5m, 16 cylindrical obstacles distribute in the circle of R = 10m, 24 cylindrical obstacles distribute in the circle of R = 15m, and 32 cylindrical obstacles distribute in the circle of R = 20m ($\text{MCY}_4$).

The models of the middle deck offshore oil platform with different quantities of obstacles of varying volumes are established by AutoReaGas software. The perimeter of each model is setting an "open" boundary, and the top and bottom surfaces are set as "solid" boundaries to simulate platform decks. Five gauged points are located along the $y$ axis, and their coordinates in the established coordinate system are gauge 1 $(0, 0, 2.25)$, gauge 2 $(0, 0, 7.25)$, gauge 3 $(0, 0, 12.25)$, gauge 4 $(0, 0, 17.25)$ and gauge 5 $(0, 0, 22.25)$. The gauged points and boundaries are shown in Figure 3 and the computational domain is divided

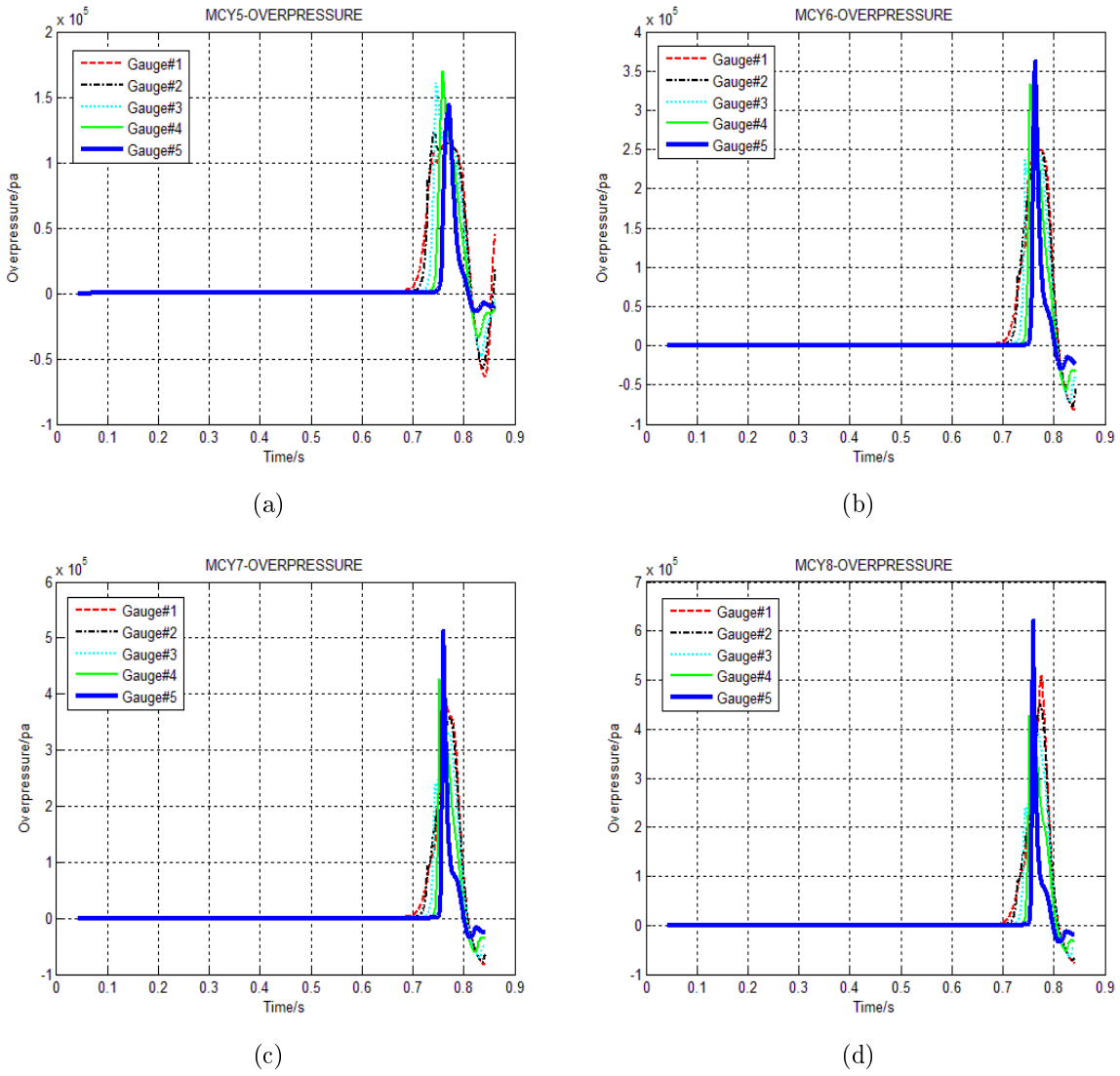


FIGURE 6. The overpressure is influenced by the quantities of cylindrical obstacles and the volume of each is 15.9m$^3$. (a) 8 obstacles distribute in the circle of R = 5m ($MCY_5$), (b) 8 cylindrical obstacles distribute in the circle of R = 5m, and 16 cylindrical obstacles distribute in the circle of R = 10m ($MCY_6$), (c) 8 cylindrical obstacles distribute in the circle of R = 5m, 16 cylindrical obstacles distribute in the circle of R = 10m, and 24 cylindrical obstacles distribute in the circle of R = 15m ($MCY_7$), (d) 8 cylindrical obstacles distribute in circle of R = 5m, 16 cylindrical obstacles distribute in the circle of R = 10m, 24 cylindrical obstacles distribute in the circle of R = 15m, and 32 cylindrical obstacles distribute in the circle of R = 20m ($MCY_8$).

into 25000 grids. In order to maintain high accuracy, the primary computational grid density in the direction of the $z$-axis is doubled by halving the $z$-dimension of otherwise cubic cells, resulting in computational cells of 1m × 1m × 0.5m.

3.2. **Working conditions of simulation.** In order to simulate and find the relation between peak overpressure and temperature in different obstructed environments and volumetric blockage ratios of offshore oil platforms, this article selects 4 grouped quantities

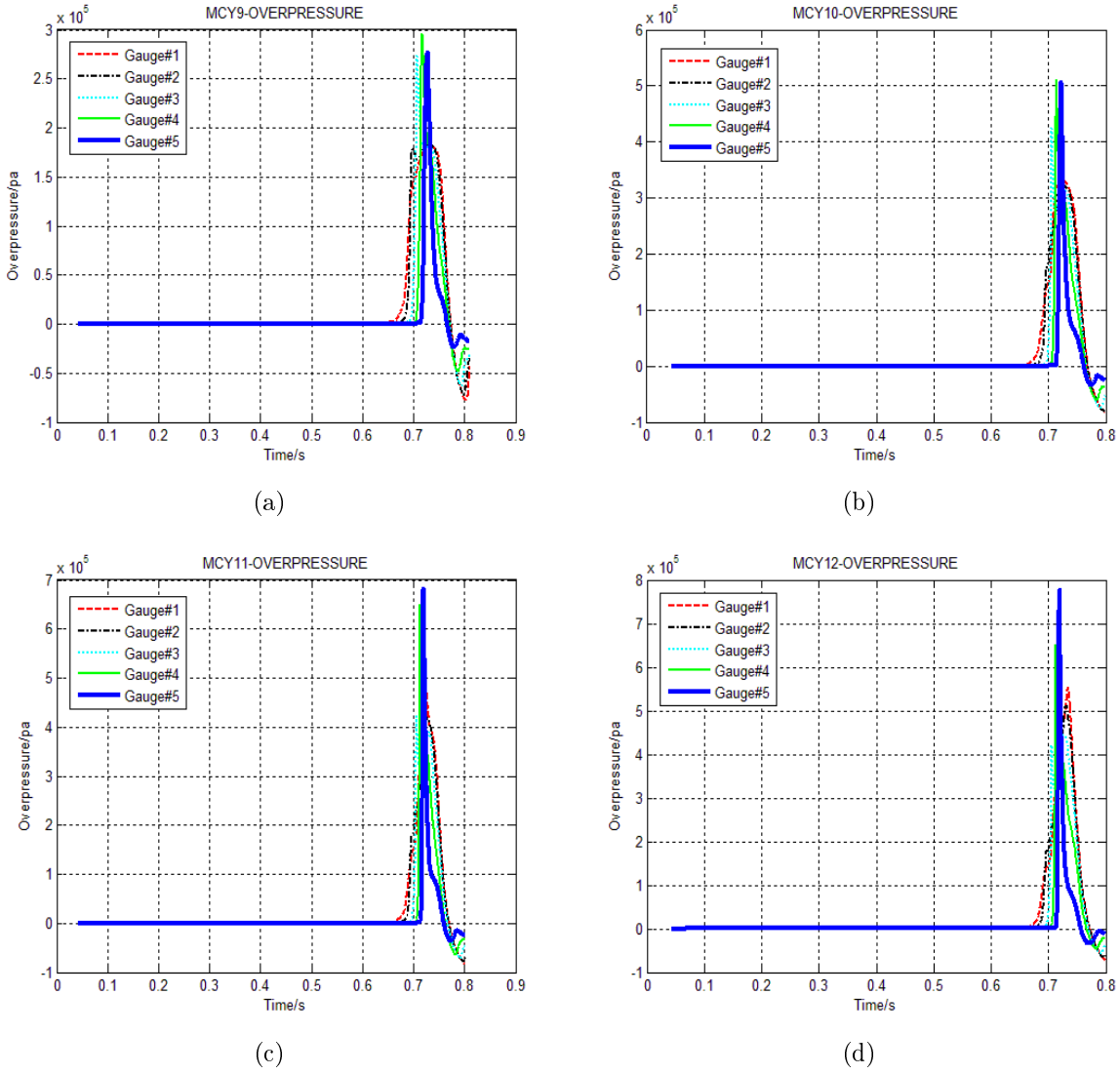


FIGURE 7. The overpressure is influenced by the quantities of cylindrical obstacles and the volume of each is 34.9m$^3$. (a) 8 obstacles distribute in the circle of R = 5m (MCY$_9$), (b) 8 cylindrical obstacles distribute in the circle of R = 5m, and 16 cylindrical obstacles distribute in the circle of R = 10m (MCY$_{10}$), (c) 8 cylindrical obstacles distribute in the circle of R = 5m, 16 cylindrical obstacles distribute in the circle of R = 10m, and 24 cylindrical obstacles distribute in the circle of R = 15m (MCY$_{11}$), (d) 8 cylindrical obstacles distribute in the circle of R = 5m, 16 cylindrical obstacles distribute in the circle of R = 10m, 24 cylindrical obstacles distribute in the circle of R = 15m, and 32 cylindrical obstacles distribute in the circle of R = 20m (MCY$_{12}$).

of cylindrical obstacles and 3 different values for volume. The selected cylindrical obstacles are the most common in the layout of actual offshore oil platforms. Each grouped quantity is paired with one of the three selected volumes which, along with a control condition of zero obstructions, results in a total of 13 working conditions. In Figure 2, it is shown that obstacles are placed in rings of radii 5m, 10m, 15m, or 20m. Since obstacles remain equidistant, the 5m ring can fit exactly 8 obstacles, the 10m ring can fit 16, etc. Each ring is represented in a separate column in Table 2.

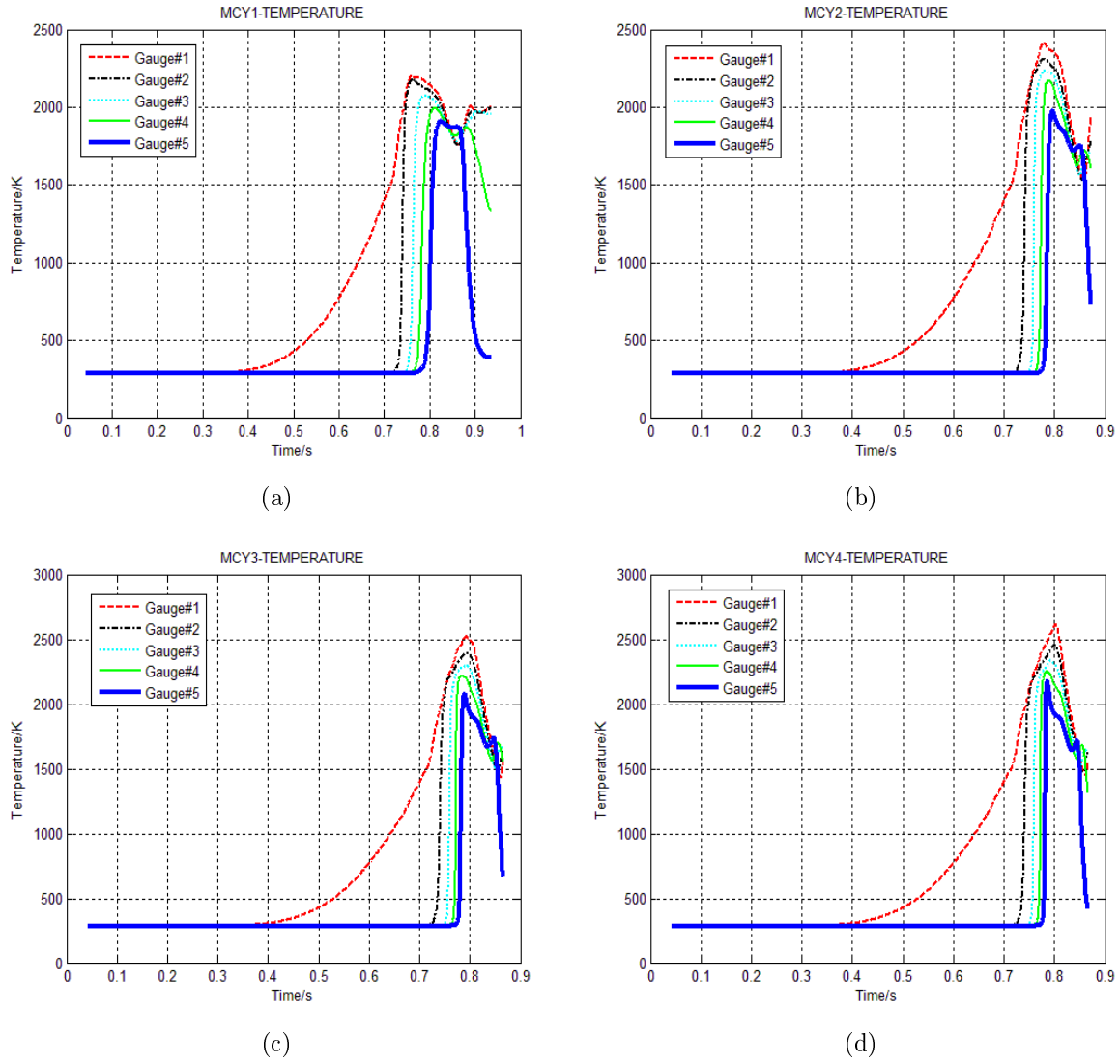


FIGURE 8. The temperature is influenced by different quantities of cylindrical obstacles and the volume of each is $3.9\text{m}^3$. (a) The relationship between the temperature and time of $\text{MCY}_1$, (b) the relationship between the temperature and time of $\text{MCY}_2$, (c) the relationship between the temperature and time of $\text{MCY}_3$, (d) the relationship between the temperature and time of $\text{MCY}_4$.

4. **Results and Discussion.** In this section, the results of thirteen simulation working conditions are discussed.

4.1. **Simulative results without any obstacle.** In order to research the influence of peak overpressure and temperature by obstacles, the result without any obstacle is simulated in Figure 4. The peak overpressure is 375pa and it appears at 1.2s while the peak temperature is 2089K and it appears at 2s.

4.2. **Simulative results of overpressure with cylindrical obstacles.** The range of peak overpressure in Figure 5 is from $8.1\times10^4$pa to $3.4\times10^5$pa, Figure 6 is from $1.7\times10^5$pa to $6.2\times10^5$pa, and Figure 7 is from $3.0\times10^5$pa to $7.8\times10^5$pa. These are all much larger values than those of the working condition without obstacles. With increasing quantities of cylindrical obstacles, the peak overpressure increases. The time at which peak value

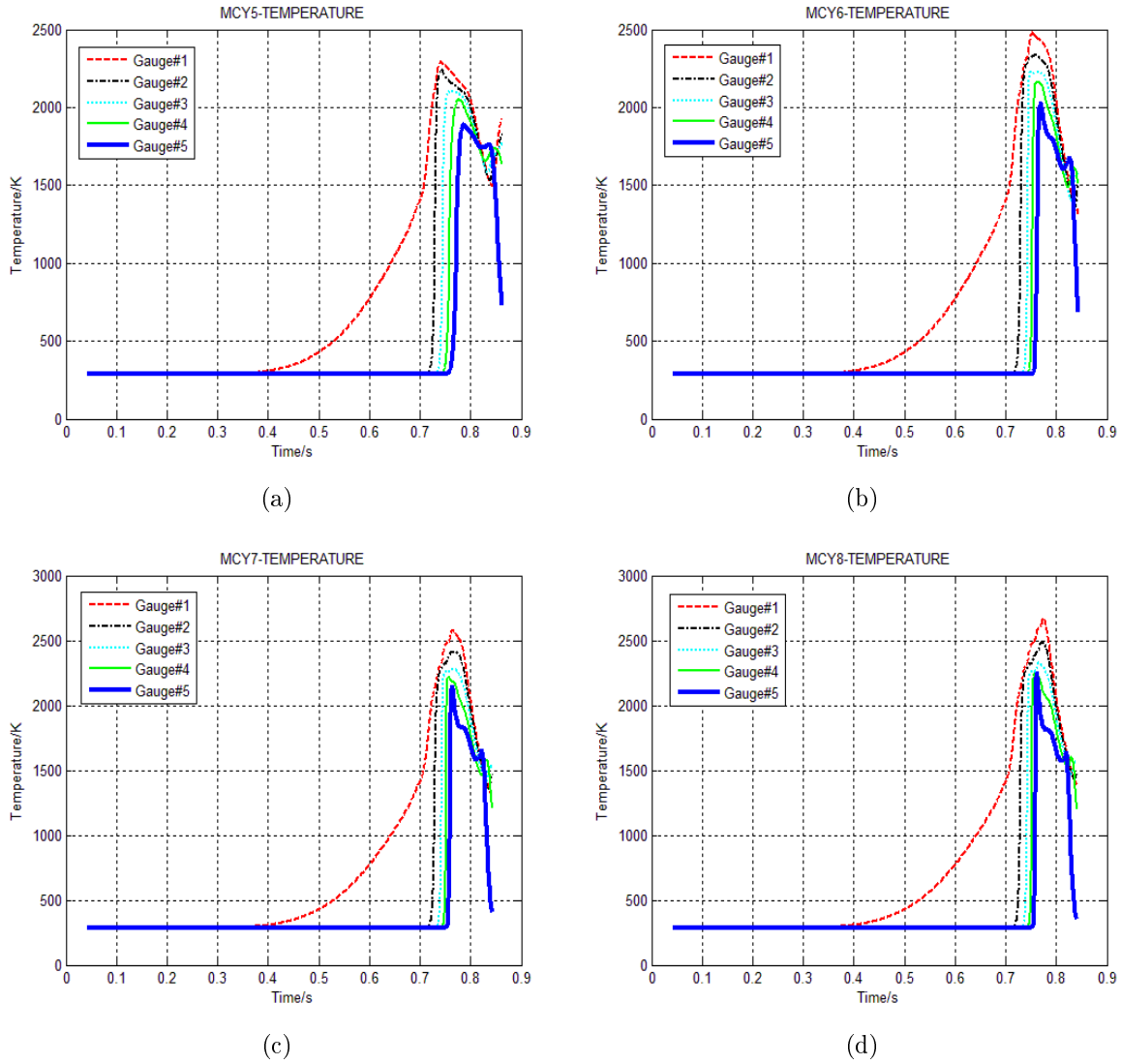


FIGURE 9. The temperature is influenced by different quantities of cylindrical obstacles and the volume of each is 15.9m$^3$. (a) The relationship between the temperature and time of MCY$_5$, (b) the relationship between the temperature and time of MCY$_6$, (c) the relationship between the temperature and time of MCY$_7$, (d) the relationship between the temperature and time of MCY$_8$.

is achieved remains within the 0.7s to 0.8s range. The phenomenon is caused by the inducing effect of cylindrical obstacles, which accelerates the shockwave at a high rate and reach peak overpressure in a shorter amount of time.

4.3. **The simulative results of temperature with cylindrical obstacles.** The following figures (Figure 8/Figure 9/Figure 10) show that the peak temperature appears within 0.8s which is much less than that of the working condition without any obstacles. The reason is that obstacles can change the laminar combustion to turbulent combustion in a short amount of time, and the rate of propagation of the flame is much quicker. The combustion rate is also higher.

4.4. **The discussion of peak overpressure and peak temperature.** It is obvious that the cylindrical obstacles contribute to increasing peak overpressure and temperature.

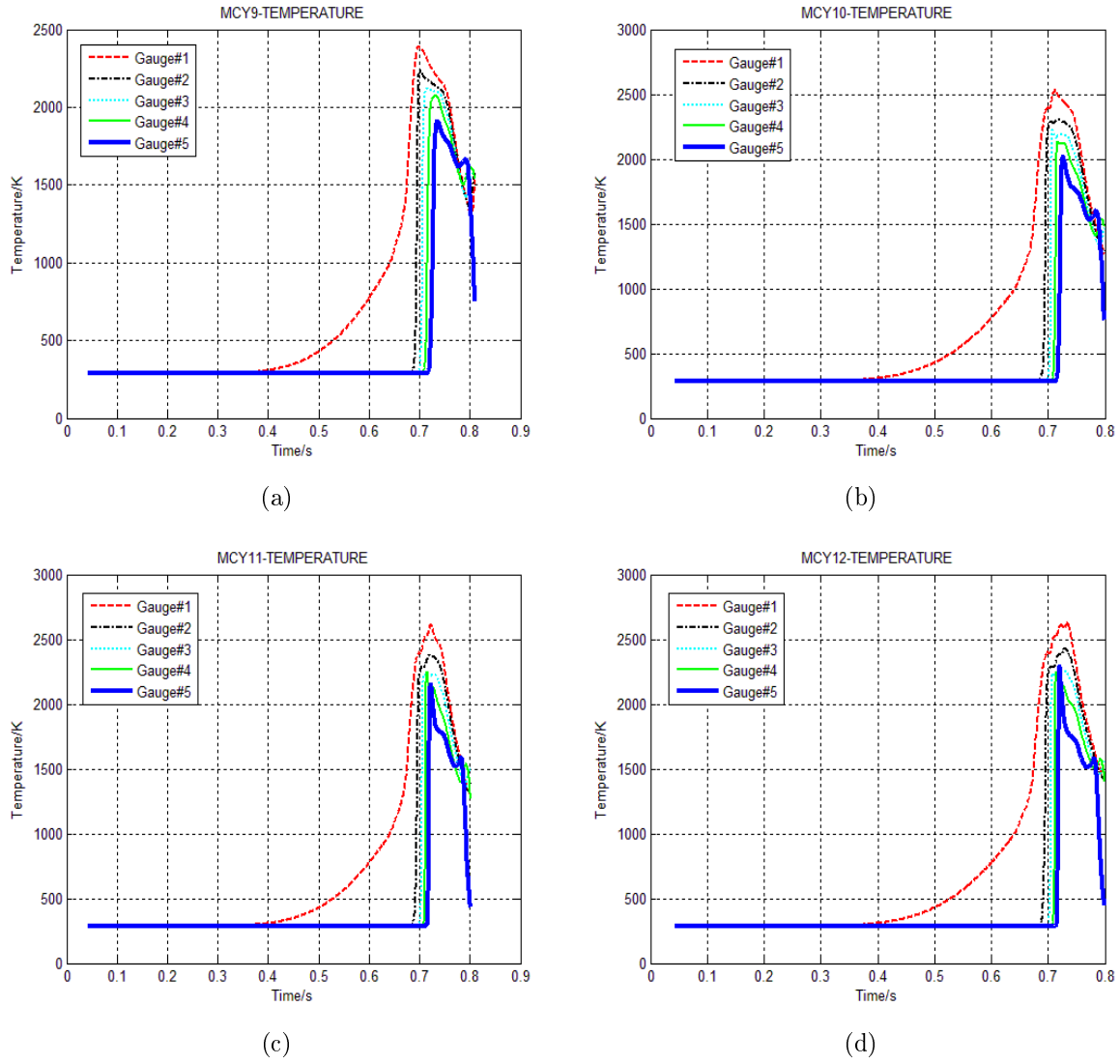


FIGURE 10. The temperature is influenced by different quantities of cylindrical obstacles and the volume of each is 34.9m$^3$. (a) The relationship between the temperature and time of MCY$_9$, (b) the relationship between the temperature and time of MCY$_{10}$, (c) the relationship between the temperature and time of MCY$_{11}$, (d) the relationship between the temperature and time of MCY$_{12}$.

In order to find the rules of how peak overpressure and temperature are influenced by these cylindrical obstacles in the middle deck of the offshore oil platform, the simulative results of peak overpressure are compared in Figure 11 and peak temperature in Figure 13. These two charts have the same volumes for each of the cylindrical obstacles but differ in quantity. In addition, simulative results of peak overpressure are compared in Figure 12 and peak temperature in Figure 14. These two charts have the same obstruction quantities but the obstructions vary by volume.

4.4.1. *Comparison of peck overpressure.* Figure 11 shows that in a lower volumetric blockage ratio (a), the peak overpressure in gauged points increases with the quantity of cylindrical obstacles. The increasing range firstly decreases and then increases. Furthermore, in medium (b) and higher volumetric blockage ratio (c), the peak overpressure in gauged

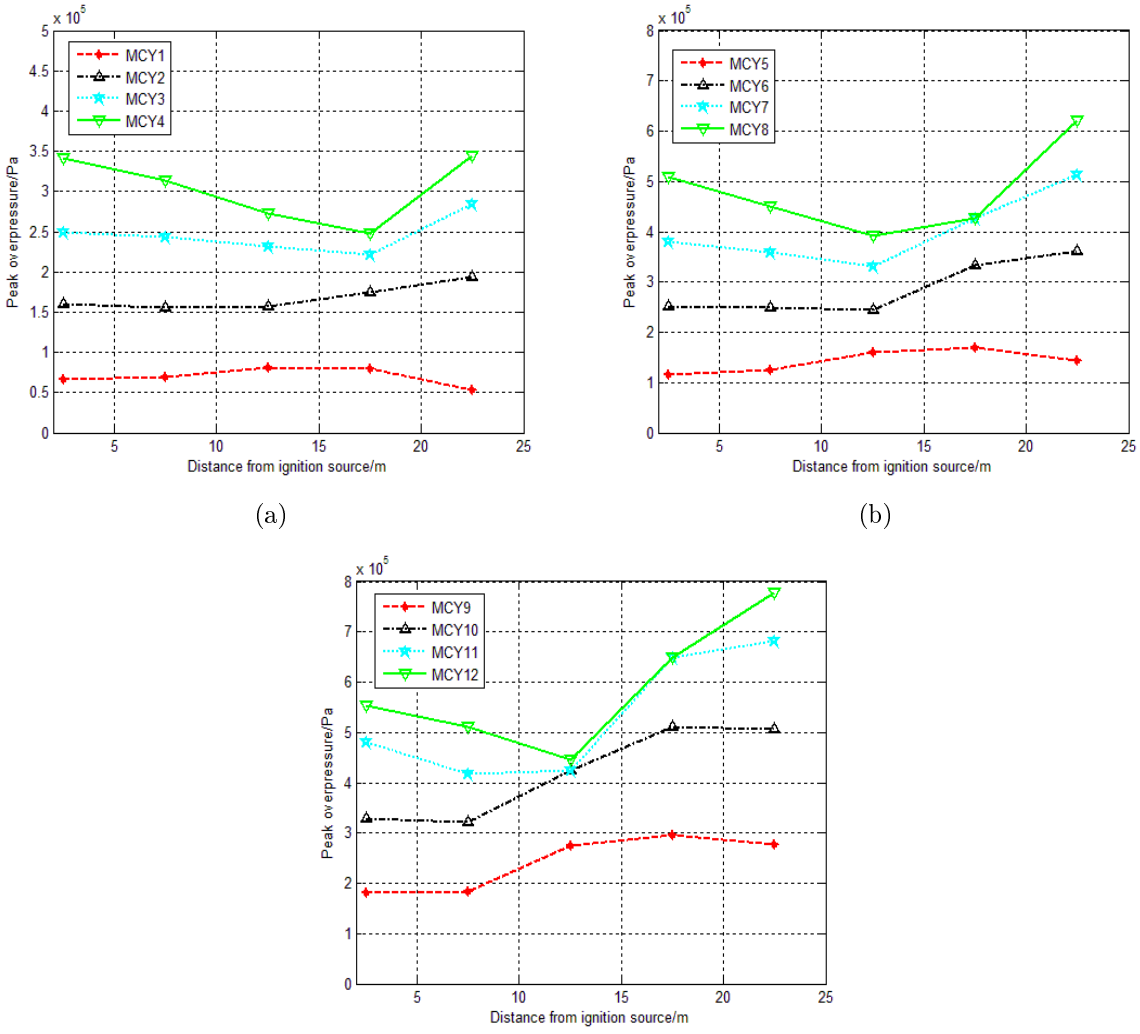


FIGURE 11. The relationship between the peak overpressure and the distance from ignition source of gauged points, which have the same obstructed volume of each but different quantities. (a) Each volume is 3.9m$^3$, (b) each volume is 15.9m$^3$, (c) each volume is 34.9m$^3$.

points generally increases with the quantity of cylindrical obstacles except gauge 3 and gauge 4 (appeared coincident point). Comparing with (a), (b) and (c) the rules are found that the coincident trend appears in different gauged points, and the coincident trend in gauged points is closer to the ignition source when the volumetric blockage ratio is larger. A corollary also can be deduced that with the increase in volumetric blockage ratio, the effect of obstructed quantities declines. Figure 12 shows the peak overpressure in gauged points, which increases with the volumetric blockage ratios of cylindrical obstacles. Furthermore, when the cylindrical obstacles are sited at the circles of R = 5m only and R = 5m plus R = 10m, the peak overpressure increases with the distance from ignition source; when the cylindrical obstacles are sited at the circles of R = 5, R = 10m, R = 15m and R = 5m, R = 10m, R = 15m, R = 20m, the peak overpressure firstly decreases and then increases along the distance from ignition source.

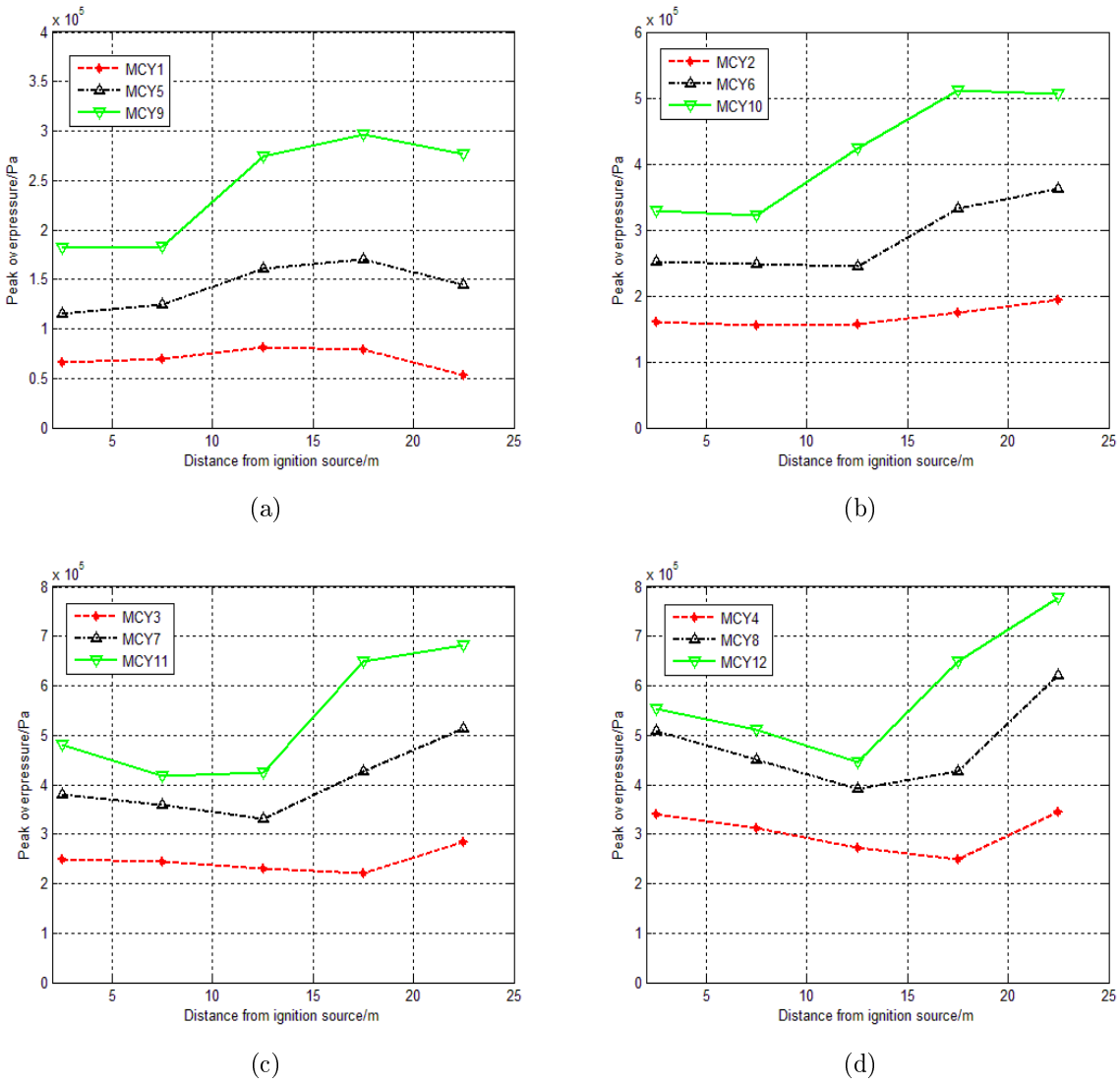


FIGURE 12. The relationship between the peak overpressure and the distance from ignition source of gauged points, which have the same obstacles but different volumes of each obstacle. (a) Total quantities of obstacles are 8, (b) total quantities of obstacles are 24, (c) total quantities of obstacles are 48, (d) total quantities of obstacles are 80.

4.4.2. *Comparison of peak temperature.* Figure 13 shows that the peak temperature in gauged points increases with the quantity of cylindrical obstacles and decreases with respect to the distance from the ignition source. The range of peak temperatures is about 1900K to 2700K. Figure 14 shows that the peak temperature in gauged points moderately increases with a rise in volumetric blockage ratio when the quantity of cylindrical obstacles is 8. Peak temperature in the gauged points is approximately the same, separately shown in (b), (c) and (d), which implies that the change of volumetric blockage ratio has modest influence on peak temperature, usually amplitudes of less than 100K when measured at the gauge points.

5. **Conclusions.** In the present work, the study aims at finding relationship of natural gas explosions between peak overpressure/temperature and cylindrical obstacles. The methodology of finite elements was used in constructing models of natural gas explosions in

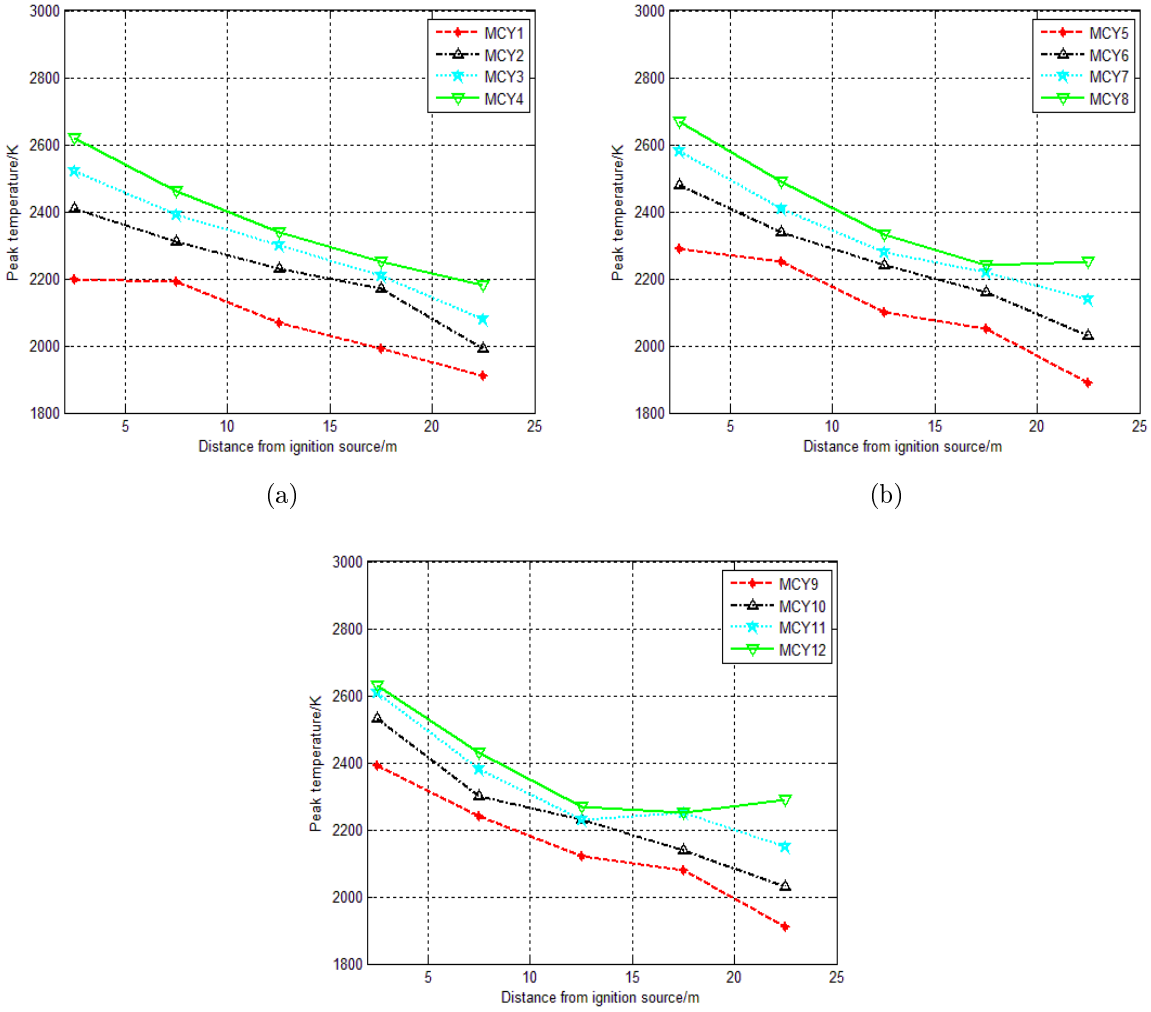


FIGURE 13. The relationship between the peak temperature and the distance from ignition source of gauged points, which have the same obstructed volumes of each but different quantities. (a) Each volume is 3.9m$^3$, (b) each volume is 15.9m$^3$, (c) each volume is 34.9m$^3$.

combination with a simulation of working conditions. These conditions have been devised in order to simulate the common shape of cylindrical obstacles and factors influencing the peak overpressure/temperature, such as quantity of obstacles the volumetric blockage ratio. The study shows that comparing with an explosion that has no obstacles around it, the effect of cylindrical obstacles increases the peak pressure/temperatures significantly. The peak overpressure increases with the volumetric blockage ratio of cylindrical obstacles, but with an increase in the volumetric blockage ratio, the overall effect of the obstacles' quantity decreases. The peak temperature in gauged points increases with the quantity of cylindrical obstacles and generally decreases along the distance from the ignition source. The range of peak temperature is between 1900K to 2700K. If obstacles are not less than eight, changes in the volumetric blockage ratio make little influence on temperature with an amplitude less than 100K. These rules of peak overpressure and temperature can be used to optimize the layout of offshore oil platforms, which could reduce the damage in natural gas explosion accidents. The further study on finding the balance point between

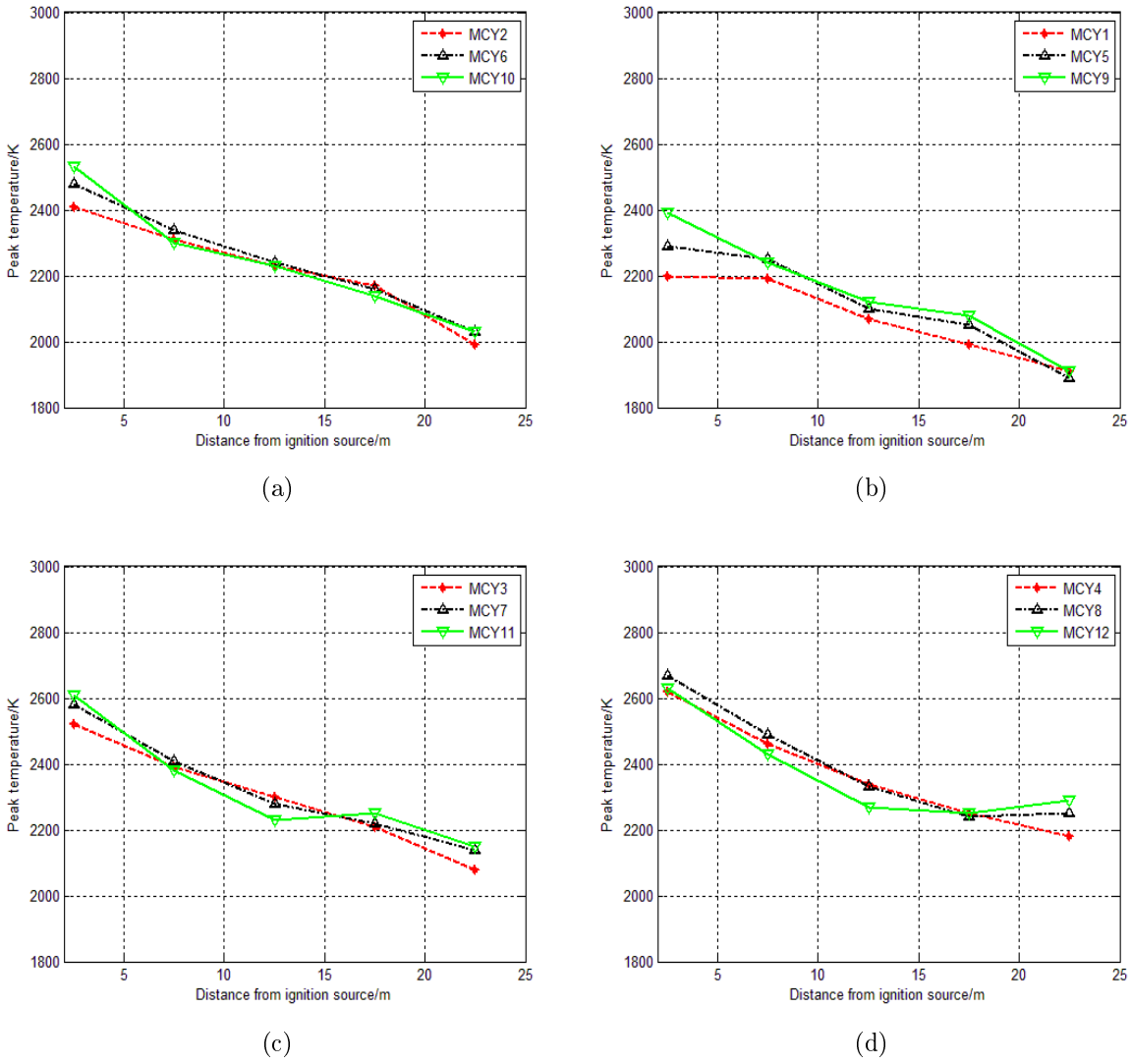


FIGURE 14. The relationship between the peak temperature and the distance from ignition source in gauged points, which have the same quantities of obstacles but different volume of each. (a) Total quantities of obstacles are 8, (b) total quantities of obstacles are 24, (c) total quantities of obstacles are 48, (d) total quantities of obstacles are 80.

volumetric blockage ratio and the volume of flammable gas in the middle deck of offshore oil platform is needed.

## REFERENCES

[1] C. J. Hayhurst, N. J. Robertson, K. C. Moran, R. A. Clegg and G. E. Fairlie, Gas explosion and blast modeling of an offshore platform complex, *Proc. of the ERA Conference on Fire and Explosion Engineering*, London, UK, 1998.

[2] X. D. Li, C. H. Bai and Q. M. Liu, Effects of obstacles on flame propagation behavior and explosion overpressure development during gas explosions in a large closed tube, *Journal of Beijing Institute of Technology*, vol.16, no.4, pp.399-403, 2007.

[3] S. S. Ibrahim and A. R. Masri, The effects of obstructions on overpressure resulting from premixed flame deflagration, *Journal of Loss Prevention in the Process Industries*, vol.14, no.3, pp.213-221, 2001.

[4] E. Salzano, F. S. Marra, G. Russo and J. H. S. Lee, Numerical simulation of turbulent gas flames in tubes, *Journal of Hazardous Materials*, pp.233-247, 2002.
[5] Q. Zhang, L. Pang and H. M. Liang, Coupling relation between air shockwave and high-temperature flow from explosion of methane in air source, *Flow Turbulence and Combustion*, vol.89, no.1, pp.1-12, 2012.
[6] W. P. M. Mercx, A. C. Berg, C. J. Hayhurst, N. J. Robertson and K. C. Moran, Developments in vapour cloud explosion blast modeling, *Journal of Hazardous Materials*, pp.301-309, 2000.
[7] L. Pang, Q. Zhang, T. Wang, D. C. Lin and L. Cheng, Influence of laneway support spacing on methane/air explosion shock wave, *Safety Science*, no.50, pp.83-89, 2012.
[8] A. Graham, C. Edmund and P. David, Patel Jacqueline explosion risks at small LNG sites, *Institution of Chemical Engineers Symposium Series*, vol.2015, no.160, 2015.
[9] B. Fan, C. Bai and B. Li, Numerical simulation of overpressure field of gas explosion in confined roadway, *Beijing Ligong Daxue Xuebao/Transaction of Beijing Institute of Technology Academic Journal*, vol.33, no.2, pp.97-100, 2013.
[10] N. K. Shetty, C. G. Soedes, P. Thoft et al., Fire safety assessment and optimal design of passive fire protection for offshore structures, *Reliability Engineering & System Safety*, vol.61, nos.1-2, pp.139-149, 1998.
[11] B. Y. Jiang, B. Q. Lin, S. L. Shi et al., Numerical analysis on propagation characteristics and safety distance of gas explosion, *Procedia Engineering*, no.26, pp.271-280, 2001.
[12] B. Jang, B. Lin, S. Shi, C. Zhu and J. Ning, Numerical simulation on influence of initial temperature and initial pressure on attenuation characteristic an safety distance of gas explosion, *Combustion Science and Technology*, vol.184, pp.135-150, 2012.
[13] K. N. C. Bray, Studies of the turbulent burning velocity, *Proc. of the Royal Society of London*, vol.A431, pp.315-325, 1990.